

# Accurate determination and correction of the lattice parameter of LaB<sub>6</sub> (standard reference material 660) relative to that of Si (640b)

C. T. Chantler,\* N. A. Rae and C. Q. Tran

School of Physics, University of Melbourne, Victoria 3010, Australia. Correspondence e-mail: chantler@ph.unimelb.edu.au

X-ray powder diffraction and synchrotron radiation have been used to determine the lattice parameter of the NIST standard reference material (SRM 660) LaB<sub>6</sub> as 4.156468 Å with an accuracy of 12 parts per million (p.p.m.), calibrated relative to the lattice parameter of the Si powder standard [ $a_0 = 5.430940(11)$  Å, Si 640b]. A discrepancy of 0.00048 (5) Å, or nine standard deviations from the NIST reference, is observed between the currently accepted lattice spacing of LaB<sub>6</sub> and the measured value. Twelve different measurements of the lattice parameter were made at beam energies between 10 and 20 keV. The observed discrepancy in the lattice parameter is consistent for the different energies used. The absolute values of the mean difference between the measured and calculated  $2\theta$  centroids,  $|\overline{\delta 2\theta}|$ , are highly consistent, between 0.0002 and 0.0004° for energies from 5 to 14 keV, and between 0.0005 and 0.0008° for energies from 15 to 20 keV. In order to determine the peak positions with high precision, account must be taken of the observed peak asymmetry. It is shown that significant asymmetry is due to peak broadening and must be taken into account in order to determine accurate peak locations and lattice spacings. The approach shows significant advantages over conventional analysis. The analysis of peak broadening is compared with models used in Rietveld analysis.

© 2007 International Union of Crystallography  
Printed in Singapore – all rights reserved

## 1. Introduction

Powder diffraction is a commonly used technique in synchrotron studies for characterizing materials (see, for example, Ávila-Godoy *et al.*, 2006). The high intensity of the beam, the relative simplicity of the X-ray optics and the tunability of wavelength from synchrotron sources widens the applicability to powder diffraction techniques. For the determination of accurate lattice parameters and to reduce possible correlated uncertainties, it is common to make use of a standard powder sample whose lattice parameter is well known. For this purpose, the National Institute of Standards and Technology has defined Standard Reference Materials (SRMs). The 640 and 660 series SRMs are the most accurate powder standards available:  $a_0 = 5.430940(11)$  Å for silicon 640b (Parrish *et al.*, 1999) and  $a_0 = 4.15695(6)$  Å for lanthanum hexaboride 660 (Rasberry *et al.*, 1989).

We used these two SRMs to determine the beam energies from the known lattice parameters in an X-ray attenuation measurement of silver, copper and gold, carried out across the energy range from 5 to 20 keV (Chantler *et al.*, 2001, 2003). In the course of this analysis, we noted a systematic discrepancy due to a small error in the ratio of the Si 640b and LaB<sub>6</sub> 660 lattice parameters (Chantler *et al.*, 2004). In a new series of measurements, we have collected much better statistics across a range of energies to reinvestigate this discrepancy. Powder

patterns were recorded for both powders at each energy and analyzed to determine the beam energy to better than 0.025% at all energies (Rae *et al.*, 2006). This paper now investigates the discrepancy in the lattice parameters. Since the quoted uncertainty in the Si 640b lattice parameter is five times smaller than that for LaB<sub>6</sub> 660, we report a correction of the LaB<sub>6</sub> lattice parameter relative to the accepted value of the lattice parameter of Si 640b (Parrish *et al.*, 1999).

In this paper we explain the basis of the analysis and prove the high quality of the data for this purpose. In particular, detailed analysis reveals the importance of an understanding of the physics of the peak broadening processes. This has revealed a systematic due to the asymmetric broadening of peaks with an angle-dependent bandwidth of the synchrotron beam, which we explain and correct for. Finally, we present the results for the corrected value of the lattice parameter for LaB<sub>6</sub> 660 and discuss the significance of the result.

## 2. Experimental procedure

The Australian National Beamline Facility at the Photon Factory synchrotron is a beamline with a large powder diffractometer, BigDiff (Barnea *et al.*, 1992). Other methods including scanning goniometers with an analyser can also potentially achieve the accuracy attained in this study, but BigDiff is large and stable and well suited to standard cali-

brations. The diffraction patterns were recorded in 8 mm wide strips on six X-ray image plates covering angular ranges between approximately 15 and 160°. The image plates were mounted around the perimeter of the diffractometer as shown in Fig. 1. Radioactive fiducials on the perimeter of the diffraction chamber gave a calibrated signature for the plate locations.

In three separate experiments for copper, silver and gold attenuation, powder patterns of the Si (SRM640b) and LaB<sub>6</sub> (SRM660) standard materials (unsorted with respect to particle size) were recorded on the image plates at 23 energies between 5 and 20 keV.

Glass capillary tubes filled with the powders were spun during the exposures, resulting in smooth diffraction lines. The diameter of the tubes was 100 µm. The recorded patterns were scanned and digitized, and the fiducial markers were used to correct the 2θ values for angular offset and possible tilt of the image plates.

### 3. Analysis

Diffraction peaks were fitted with a non-linear least-squares fit of a Lorentzian convolved with a slit on a quadratic background. A simple Lorentzian or Gaussian is still useful, but a two-component profile is generally superior, especially in accounting for the tail profiles. Peak centroids were determined to a precision between 0.001 and 0.0001°, as illustrated in Fig. 2. Reduced  $\chi_r^2$  values varied from 1 to 10 for a typical energy.

The standard goodness-of-fit measure in powder diffraction studies has been the mean difference between the measured and calculated 2θ centroids for the full or selected range of peaks measured. These  $|\overline{\delta 2\theta}|$  values varied between 0.0002 and 0.0004° for energies up to 14 eV, and between 0.0004 and 0.0007° from 15 to 20 keV. This consistency should be compared with the seminal work of Hart *et al.* (1990), which obtained  $|\overline{\delta 2\theta}|$  values varying between 0.0003 and 0.0005° for energies of 9 and 12 keV after investigating only 12 reflections and omitting the Si 111 reflections. Hastings *et al.* (1984)

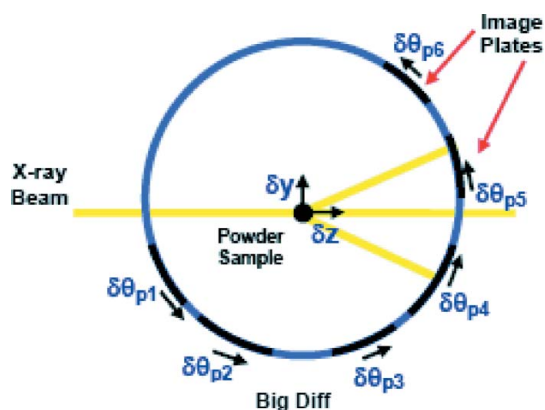


**Figure 1**

Schematic diagram of the sources of error in peak position. Image plates are mounted around the perimeter of the diffractometer of radius 57.3 cm. Each plate has an angular offset that must be fitted.

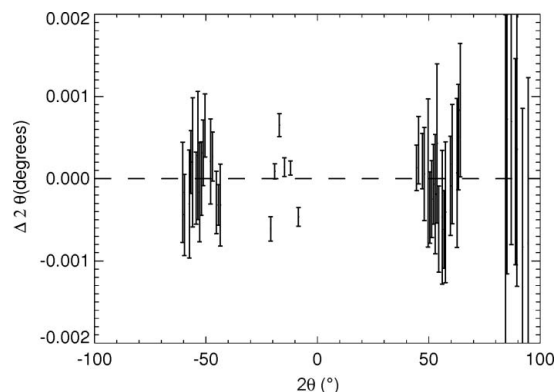


**Figure 2**

An example of lanthanum hexaboride peak angle residuals after fitting:  $E = 20$  keV, 46 peaks. Note the narrow range of residuals and the consistency within a few  $\sigma$  for each peak. Image plates have gaps between them, so not every peak is found on the four image plates used for this particular lattice determination at 20 keV. Note that the vertical scale is highly expanded compared with other literature.

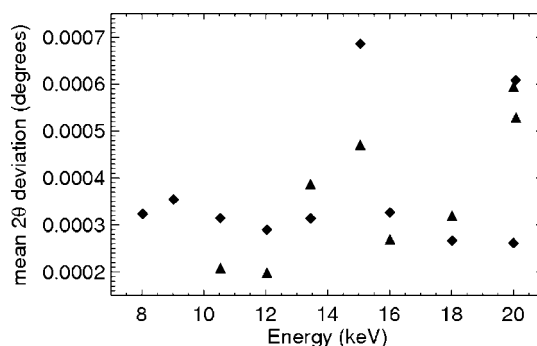


**Figure 3**

$|\overline{\delta 2\theta}|$  values varied between 0.0002 and 0.0004° for energies up to 14 eV, and between 0.0004 and 0.0007° from 15 to 20 keV. Triangles are measurements using the Si 640b standard; diamonds are measurements using the LaB<sub>6</sub> 660 standard. Consideration of each set of  $\delta 2\theta$  values for each  $|\overline{\delta 2\theta}|$  average on this plot revealed no remaining systematic structure in the residuals.

obtained  $|\overline{\delta 2\theta}|$  of approximately 0.0003°, with a zero offset error of approximately 0.03°.

Fig. 3 shows the  $|\overline{\delta 2\theta}|$  variation between the measured and calculated 2θ centroids for each experimental energy. The  $|\overline{\delta 2\theta}|$  are very small because of the high precision with which the peak central positions are determined. For all of the  $|\overline{\delta 2\theta}|$  values, there was no significant residual systematic structure in  $\delta 2\theta$ . Fig. 2 shows an example of the absence of residual systematic variation of  $\delta 2\theta$  with 2θ.

The peak angular positions are offset due to the six image-plate offsets  $\delta\theta_{pi}$  ( $i = 1$  to 6) and the eccentricity of the powder sample. The values of  $\delta\theta_{pi}$  are confirmed by the consistency of the zero position of the straight-through beam as illustrated in Fig. 4. The determined centroid position of a reflection in the positive angular region of the plates is compared with the equivalent position for the negative angular region of the plates (*i.e.* the region 0 to 90° is compared with the region 0 to -90°). Different plates do not cover the full 90° range as there

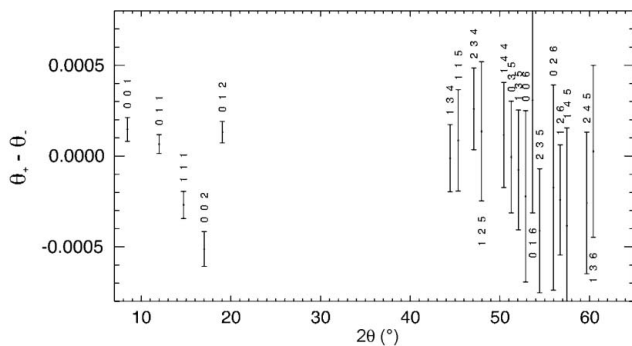


**Figure 4** LaB<sub>6</sub> test of the plate offsets and the definition of the zero position of the detector, for  $E = 20$  keV. The determined centroid position of a reflection in the positive angular region of the plates is compared with the equivalent position for the negative angular region of the plates (*i.e.* the region 0 to 90° is compared with the region 0 to -90°). All these peaks yield a consistent zero within one or two standard deviations and show that the plate offsets and zero position are well determined.

are angular offsets between the plate alignments of this diffractometer.

In this illustration, plates ‘4’ and ‘5’ have five peaks in common, while plates ‘3’ and ‘6’ have some 15 peaks in common. For each location where both positive and negative regions have yielded an accurate centroid for a peak, the mean of the two values gives the interpreted zero position of the straight-through beam, and tests this determination and the determination of the (four) plate offsets. The consistency is extremely good with no significant outlying structure and very small uncertainties.

Eccentricity of the powder sample from the centre of the diffraction chamber is characterized by a vertical offset  $\delta_y$  and a horizontal offset  $\delta_z$ . For small displacements, the corresponding angular shifts are

$$\delta\theta_y = \frac{\delta_y \cos 2\theta}{D}, \quad \delta\theta_z = \frac{\delta_z \sin 2\theta}{D}, \quad (1)$$

where  $D$  is the diameter of the diffraction chamber. These forms of  $\delta_y$  and  $\delta_z$  orthogonalize the components and minimize correlations between the two parameters. To determine the energy of the beam, we fitted the angular offset of peaks with the nominal energy  $E$  of the incident beam,

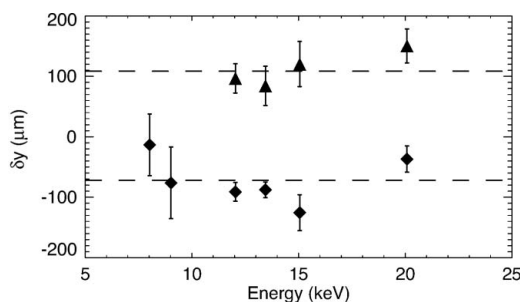


**Figure 5** Fitted vertical offset of the powder sample in  $\mu\text{m}$  versus energy for a well defined data subset. Triangle and diamond symbols are for Si and LaB<sub>6</sub>, respectively. The fitted parameters are constant across the energy range within error bars and the values are reasonable as the diameter of the sample capillary is 100  $\mu\text{m}$ .

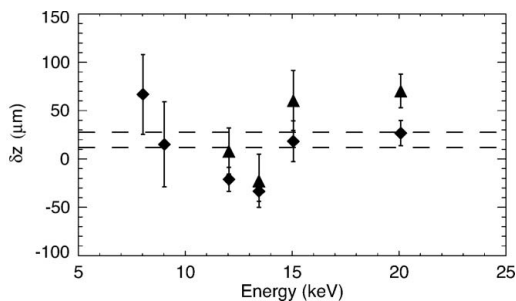


**Figure 6** Fitted horizontal offset,  $\delta_z$ , of the powder sample in  $\mu\text{m}$  versus energy. Diamonds and triangles are for Si and LaB<sub>6</sub>, respectively. The fitted parameters are reasonable as the diameters of the samples are 100  $\mu\text{m}$ . The observed offset is a possible small geometric alignment offset of the two powder goniometer head axes.

$$\arcsin\left[\frac{hc}{2d(E + \delta E)}\right] = \theta + \delta\theta_{pi} + \frac{\delta_y \cos 2\theta}{D} + \frac{\delta_z \sin 2\theta}{D}. \quad (2)$$

The vertical offset  $\delta_y$  had a significant effect on results and the offset between the powder samples (mounted on different goniometer heads) shows clearly a small 200  $\mu\text{m}$  shift between the two, due to centring of the samples (Fig. 5). The consistency of this determination within uncertainty for all energies is a strong support for the physical nature of the results.

Conversely, the horizontal offset  $\delta_z$  had a small impact on  $\chi^2_r$  and the final errors, and the results are within one standard deviation of ‘zero’ for both samples. The offset between the powder samples (mounted on different goniometer heads) is small, 15  $\mu\text{m}$ , and is within the noise (Fig. 6). The consistency of the largest coherent data set (for a silver attenuation experiment with the same powder sample and image plate location) is presented in Figs. 5 and 6. The minor variation in the value of  $\delta_z$  with energy is within one standard deviation of the mean.

This upstream/downstream shift could be expected from the increased penetration of X-rays into the silicon powder sample compared with the LaB<sub>6</sub> sample. This first-order effect would change as a function of energy (not observed) and could yield a maximum value (at low energies) of about one third of the LaB<sub>6</sub> internal capillary diameter, or about 30  $\mu\text{m}$ . This first-order effect is not observed and would be smaller than the observed differences in horizontal offset. Absorption through the powder sample therefore has negligible effect in this experiment. The consistency of this determination within uncertainty for all energies is also a strong support for the physical nature of the results.

The offset  $\delta\theta_z$  had a much smaller effect on the fitted energy than the other fit parameters. It was therefore omitted in initial analysis. Fig. 7 shows the difference between the LaB<sub>6</sub> and Si powder energy determinations from their weighted mean energy under these assumptions. This clearly indicates a consistent discrepancy between the defined lattice parameters of the materials.

There are two distinct regions in Fig. 7: below 16 keV the energy difference and error bars are smaller than from 16 to 20 keV. This difference is strongly reflected in the mean  $|\delta 2\theta|$

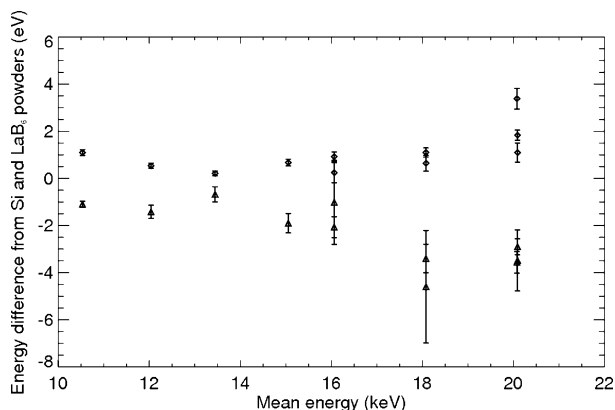


**Figure 7** Difference between  $\text{LaB}_6$  and Si powder energy determinations from their weighted mean energy, including a fitted parameter for the horizontal eccentricity of the powder position,  $\delta_z$ .  $\text{LaB}_6$  points are shown as diamonds and Si as triangles. The  $\text{LaB}_6$  points are systematically greater than the Si points by several standard deviations.

values, in Fig. 3, which implies that it is due to the input uncertainty in the peak positions.

There are nine free parameters for each energy and for each powder in this procedure. This compares, for example, to 32 data points (peak centroid locations) for the silicon powder at 20 keV in Fig. 8 and 68 independent data points (peak centroid locations) for the  $\text{LaB}_6$  powder at 20 keV in Fig. 9. The six image-plate displacements only affect peaks occurring on the given plate, while  $\delta E$  (the correction to the nominal energy),  $\delta\theta_y$  and  $\delta\theta_z$  affect all peaks. This makes it important to fit all of the peaks simultaneously, because the correlation between  $\delta\theta_y$  and  $\delta\theta_{pi}$  for each of the six image plates is different. For the data in this experiments,  $\delta\theta_z$  is sufficiently small to be neglected, reducing the number of fitting parameters.

#### 4. Peak Profile Broadening

Asymmetric broadening of peak profiles affects peak centroid positions and must be considered in a precise measurement of the peak position. Asymmetric broadening of the peak profiles will be shown to be primarily due to energy bandpass, sample size and vertical divergence. This centroid shift will be seen to be dependent upon energy and monochromation, which in a standard experiment should vary in a well defined manner. This effect has not been treated previously by other authors, and will be seen to have a significant effect upon the determination of lattice spacing, not constant for each sample or powder. In order to investigate this effect, we must model the full peak profile widths directly.

We have considered broadening due to:

- (i) the energy bandpass of the monochromated synchrotron beam;
- (ii) the powder line curvature on the imaging plate (axial divergence);
- (iii) powder sample capillary size;
- (iv) vertical beam divergence; and
- (v) image plate resolution.

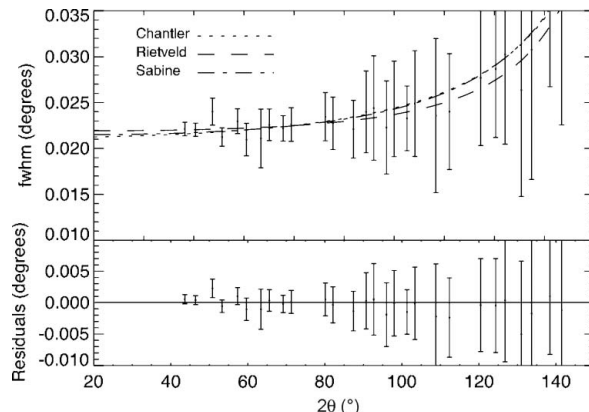


**Figure 8** Silicon FWHM  $\Delta 2\theta$  as a function of angle;  $E = 20$  keV, 32 peaks.  $\chi_r^2$  values from each fit are consistent and almost all data lie within one standard deviation of the fits. Residuals relative to the Chantler model show that the physically meaningful but simple model fully accounts for the functional dependence of the data without additional fitting parameters.

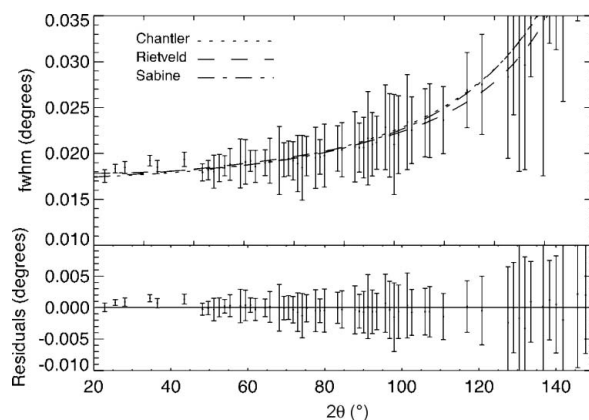


**Figure 9**  $\text{LaB}_6$  FWHM  $\Delta 2\theta$  as a function of angle;  $E = 20$  keV, 68 peaks. Error bars are consistent with Fig. 8. Residuals are relative to the Chantler model.

These are all considered below.

(vi) Additional causes of broadening including non-linear image plate response and hence dependencies upon peak intensity or bleaching of the plates with time are real effects but have no impact upon the results when linearized correctly with appropriate estimates of uncertainty from counting statistics (Cookson, 1998).

(vii) Additional causes of hypothesized broadening in some Rietveld or other modelling, such as monochromator setting, correlation between channels such as that between energy and vertical angle from the monochromator, and size or strain functions are discussed below.

Low-angle peaks with  $2\theta < 50^\circ$  were found to have significant broadening due to the curvature of the lines of the diffraction peaks when integrated over a wide linear strip (often called axial divergence). This broadening,  $\Delta 2\theta_{\text{HD}}$ , of the full width at half-maximum (FWHM) is correctly given by Sabine *et al.* (1995) as

$$(\Delta 2\theta_{\text{HD}})^2 = (0.5\Phi)^2 \cot 2\theta, \quad (3)$$

where  $\Phi$  is the angle subtended in the horizontal plane by the width of the recording strip, which was  $0.4^\circ$  for our experiment. We note in passing that this contribution is scaled by a coefficient between 0.5 and 2.0 depending upon the beam width and the alignment of the beam with the image-plate strip exposure axis. In our case, this coefficient is well approximated by 1.0, as presented by Sabine. This contribution to broadening adds in quadrature and its magnitude is fixed by the dimension of the chamber: there is no free parameter, so the effect has been removed before further processing. There is no correlation between this line curvature and the energy bandpass even if these are fitted simultaneously, because the two effects are orthogonal and affect different regions of the pattern (the high- and low-angle peaks, respectively). This low-angle broadening can be minimized by digitizing narrower strips, although this would lower statistical precision.

High-angle peaks are broadened predominantly by the energy bandpass of the beam and not by this axial divergence. The size of the powder sample, the vertical divergence of the beam, and the resolution of the plates all lead to a constant broadening of all peaks as a function of angle.

The peak FWHM values  $\Delta 2\theta$ , corrected for this fixed (primarily low-angle) broadening due to axial divergence  $\Delta 2\theta_{HD}$ , are plotted against  $2\theta$  in Figs. 8 and 9.

Three fitting functions for these data are considered in the plot. The first function considers the bandpass of the X-ray beam  $\Delta E/E$  and a constant offset  $\Delta 2\theta_0$  due to the size of the powder sample, the vertical divergence of the beam, and the resolution of the plates (Chantler *et al.*, 2004). These widths are not correlated, so must be added in quadrature:

$$(\Delta 2\theta)^2 = \left( \frac{\Delta E}{E} \tan \theta \right)^2 + (\Delta 2\theta_0)^2. \quad (4)$$

Applying equation (4) to the FWHM values for the 12 different energies resulted in consistent values for the constant and energy-dependent terms. This supports the claim that the terms are uncorrelated. Additionally, the covariance matrix determined for the fit had small off-diagonal elements, indicating the absence of correlation. The energy bandpass  $\Delta E$  was fitted to be between 2 and 6 eV (as a function of  $E$ ), which is in the typical expected range for a monochromated bending magnet X-ray beam. The uncorrelated coefficients and the physical motivation of equation (4) show that this is a good and sufficient model of these accurate data sets.

An alternate function is fitted in Figs. 8 and 9, following Sabine (1987), which takes into account the Bragg angle of the monochromator,  $\tan \theta_m$ :

$$(\Delta 2\theta)^2 = A(2m - 1)^2 + (\Delta 2\theta_0)^2 \quad (5)$$

where

$$m = \frac{\tan \theta}{\tan \theta_m}. \quad (6)$$

This function is valid; but in our experiments the negative correlation between the monochromator angle and the powder diffraction angle (the  $-4Am$  cross-term) only yields a

low-angle broadening at or below the (single) lowest order reflection for both samples, so this formula yields almost identical fits and  $\chi_r^2$  as for the other models. We note that the coefficient  $A$  represents once again the bandpass as a function of energy.

Consider equation (4) and Figs. 8 and 9. The broadening is a function of Bragg angle for a constant energy and constant bandpass. Therefore, each profile has broadening which is symmetric from the resolution of the plates, the size of the powder sample, but there is greater broadening at higher angles from the bandpass of the monochromated beam. Hence the high-angle side of a given diffraction peak is broader than the low-angle side of the same diffraction peak. This shifts the centroid to a lower angle than the ideal position.

This is a very small asymmetry, which is perhaps why it has not been carefully considered previously. It will lead to a small error in an energy determination, and a small error in the lattice spacing determination of a single sample; but it appears that it might be the same for any sample, and hence the calibration procedure between two standards or samples such as Si and LaB<sub>6</sub> should then cancel this error and give a correct relative lattice spacing. This is not the case, as discussed in the next section.

### 5. The effect of profile asymmetry due to the bandpass

Fig. 10 models the broadening causing this correction as a function of angle for a specific bandpass (2 eV Gaussian FWHM) and a specific synchrotron energy (15 keV). This function is smooth and well behaved for any given powder sample (*e.g.* silicon or LaB<sub>6</sub>) and for any given energy; however, for a particular energy, the distribution of diffraction peaks as a function of angle leads to differences in the mean effect of this broadening asymmetry. Because the distribution

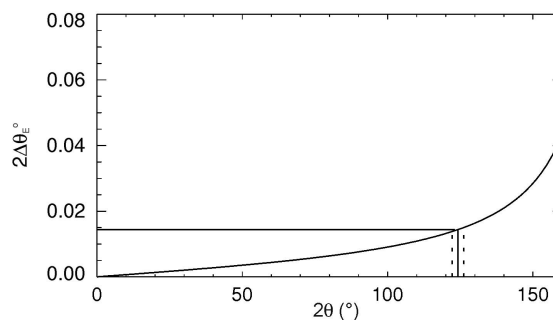


**Figure 10** The contribution to the peak profile width from the Gaussian model function of the 2 eV FWHM bandpass broadening for a synchrotron beam energy of 15 keV. The model function width varies with angle and especially affects the higher angle peak locations. The dotted lines show two points on the low- and high-angle sides of the designated peak from which the derivative of the curve can be computed for the relevant Bragg angle (Fig. 11). The broadening of the experimental data peaks is given by the slope (derivative) of the FWHM as a function of angle, for a given energy and bandpass. The slope and width around the peak gives the centroid shift from the effect upon the amplitude. Although the corresponding centroid shift is barely distinguishable, the functional form of this shift has a significant impact upon the final results.

of high- and low-angle peaks differs between any two samples or standards, this leads to an overall correction in the comparison of one with another.

This profile asymmetry was corrected by a point-wise deconvolution of a Lorentzian with width given by equation (4). The asymmetric broadening shifts the peak to lower angles, although the high-angle tail extends further. For high angles, this leads to an overall centroid shift to lower angles, as illustrated by Fig. 10.

To consider this illustration a little more, consider Fig. 11. Fig. 11 shows the small shift introduced by this differential asymmetry for a single peak at a given energy and angle. It is revealed more in the small change in the centroid rather than the minor profile asymmetry of the broadened profile.

The overall width of the peak is *ca*  $0.047^\circ$  and the deconvolving width is *ca*  $0.02^\circ$ . Hence the fitted profile after deconvolution is narrower (and has a higher peak amplitude) than the full or convolved peak (the original data). The centroid shift is always a small fraction of the deconvolving width, and depends upon the quality of the data and the magnitude of the slope asymmetry of the broadening function. In this example and at this relatively high angle, a centroid shift of  $0.0005^\circ$  is typical, and only one fortieth of the deconvolving width.

This shift seems very small, is significantly less than the standard deviation reported by the fit, and is similar for both samples at these angles. At lower angles, the typical shift is much smaller still. However, the net effect of fitting these results is up to a  $2\sigma$  change of the overall lattice parameter for particular energies, noting of course that our standard error for a given energy is quite a small number (see §7).

This correction, when implemented, improved the reproducibility of the discrepancies obtained for each and every energy. Above 16 keV it reduced the uncertainty for a given energy; and below 16 keV the discrepancy between the lattice spacings became more consistent. The point-wise deconvolution tends to increase the noise in a given peak and hence the scatter of results for a particular distribution, but the trend and dominant signature is given by the formula and by Fig. 10. The uncertainty in the lattice-parameter measurement at a given

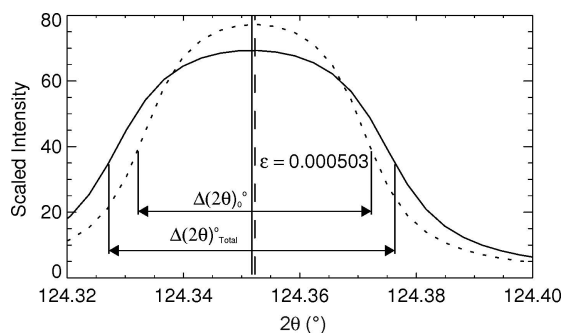


**Figure 11**

Profiles of typical fitted peaks for the measured and point-wise deconvolved peak after removing a Gaussian for 2 eV FWHM, a synchrotron beam energy of 15 keV and a Bragg angle of  $124.35^\circ$ . The full line shows the unbroaderened profile and its centroid and the dotted line shows the asymmetrically broadened profile and its centroid as observed in the data. The difference is the centroid shift  $\epsilon$  as indicated on the plot.

energy increases because of the scatter, but the results at different energies become more uniform.

In the data sets that are uncorrected for this profile asymmetry, the high-energy results are clearly inconsistent with the central energy results, and the error bars of the high-energy data do reflect this. The asymmetry discussed is larger and less well determined at these higher energies, because the distribution of reflections with angle shifts towards higher angles and there is greater noise on individual high-angle peaks. Hence the well determined central energies were selected for further analysis (the eight 'less than 16 keV' data in the plots). Subsequent checks and refitting showed that inclusion of the other energies yields larger scatter, but does not change the sign or magnitude of the discrepancy observed. Analysis of this subset therefore reduces both random scatter (because of the poorer statistics at the higher energies) and a larger, less well defined systematic error.

## 6. Consistency of the fitting results

The fitting parameters in equation (2) are consistent across the energy range and have physically reasonable values. For example, Fig. 6 shows the vertical powder eccentricity. The values are constant with energy within error bars. The  $\text{LaB}_6$  powder has a different value for  $\delta\theta_y$ , compared with Si; however, this is to be expected, as the two powder samples are mounted on two different goniometer heads. The value of between  $50\ \mu\text{m}$  and  $100\ \mu\text{m}$  is less than the error in alignment and is comparable with the diameter of the capillary. It is therefore a physically reasonable parameter. This suggests that the fitted  $\delta\theta_y$  parameter is well fitted and that the fitting parameters are not unreasonably correlated.

The fitting procedure was repeated including  $\delta\theta_z$ . Fig. 6 shows the fitted  $\delta\theta_z$  values for the different experimental energies. As with Fig. 5, the values are consistent with a value independent of energy and are physically reasonable. This parameter  $\delta\theta_z$  was a higher order effect than the plate offset and vertical eccentricity of the powder sample; *i.e.* it was not so significant, and so was included in a re-analysis. Its inclusion in the fitting procedure leads to reduction in the  $1\sigma$  error bars in Fig. 7 and a small change to the fitted energy, within the standard deviation of the initial determination. Fig. 7 shows the difference between  $\text{LaB}_6$  and Si powder energy determinations after including the fitting of  $\delta\theta_z$ . It can be seen that both approaches are consistent, robust and convergent with high-quality data.

## 7. Lattice-parameter determination

A measurement of the  $\text{LaB}_6$  lattice parameter relative to the Si standard was obtained by comparing the energy determinations at the same energy by the two powder patterns. Since the quoted standard deviation in the SRM lattice parameter for Si 660b is much less than for  $\text{LaB}_6$ , the Si lattice parameter was used to obtain the  $\text{LaB}_6$  lattice parameter. At eight different X-ray wavelengths, the obtained lattice parameter of  $\text{LaB}_6$  was consistently higher than the SRM reference

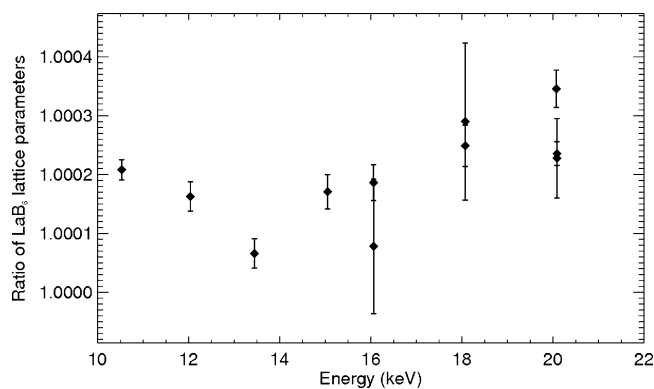


**Figure 12** Ratio of SRM LaB<sub>6</sub> lattice parameter and the measured value at each energy, including a fitted parameter for  $\delta_z$ . The ratio is determined separately at each energy and is consistent within  $2\sigma$  from 10.5 to 20 keV.

(Rasberry *et al.*, 1989). Fig. 12 shows the consistent discrepancy in the ratio of the measured lattice parameter for LaB<sub>6</sub> compared with the SRM reference lattice parameter, where the peak positions are corrected for the six plate offsets, vertical eccentricity of the powder sample and a shift in the energy of the beam. The consistency of the sign of the difference between the powder determinations is a strong case for the conclusion that the LaB<sub>6</sub> lattice parameter is discrepant, and this result strongly confirms the trend reported by Chantler *et al.* (2004).

The lattice-parameter determination has been corrected for thermal expansion, as given by Chantler *et al.* (2004). The correction (and the uncertainty in the correction) is an order of magnitude smaller than the observed discrepancy.

Horizontal eccentricity of the powder sample,  $\delta\theta_z$ , was not included in the procedure used to calculate ratios shown in Fig. 12. Its inclusion in the energy determination had the effect of slightly increasing the difference between values measured for the two powders, while reducing the error in the value, as can be seen in Fig. 7. It therefore leads to an increase in the determined lattice parameter discrepancy. This shift is less than 1.5 standard deviations, and hence we can consider equally the merits of the two alternate analyses.

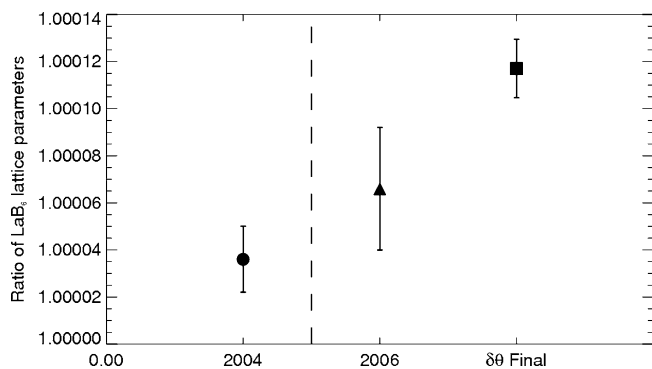


**Figure 13** Corrections to the LaB<sub>6</sub> lattice parameter, both including and excluding the broadening correction, and compared with the correction reported by Chantler *et al.* (2004).

Fig. 13 shows the average over energy of the measured LaB<sub>6</sub> ratio and SRM powder standard value for the value given by Chantler *et al.* (2004) uncorrected for divergence (the band-pass profile asymmetry). Compared with this baseline, the figure shows the measurements collected here, uncorrected for asymmetry and  $\delta z$ , and the final result corrected for asymmetry.

Firstly note that, without the systematic correction for asymmetry, the new data confirm our earlier measurement and conclusion to within 1.2 standard deviations. The result presented here is in agreement with the 2004 result, and confirms both the discrepancy, the sign and the magnitude. The correction for divergence (the asymmetry) increases the size of the discrepancy from the literature and in particular reduces the scatter of the independent results. This correction will generally be necessary for high-accuracy lattice determinations in the future, whether at synchrotron sources or elsewhere.

Our best estimate of the final result is the mean of the discrepancies with and without  $\delta z$  fitting, with an error bar equal to those of either method. This final result is within 1.3 standard deviations of each of these estimates and is therefore consistent with either.

Could the sample of the old standards (silicon or LaB<sub>6</sub>) be changing with time? The current determination uses a different selection of energies and more extensive reflections, but the same unsorted sample prepared in the same manner. Fig. 13 suggests that the results from this work and that of Chantler *et al.* (2004) are fully consistent when the profile asymmetry is not taken into account; that is, there is only a one standard deviation shift between the two measurements. The dominant developments in the new determination are the improved statistics, the improved analysis and the inclusion of detailed consideration of profile asymmetry and  $\delta z$  compared with the previous works. Individual energy determinations for several of the data sets are as low as 7 p.p.m. This is slightly higher than the reference determination and that of Hart *et al.* (1990), but has again had the advantage of investigating systematics involving an energy dependence, becoming a much more robust determination. This result calls for further investigation and a more accurate determination of all asymmetries in the profiles.

The asymmetry presented is very small but clearly significant, is determined accurately to first order, and increases the consistency of this high-precision data set. This asymmetry has been neglected in all previous (Rietveld) analyses of powder diffraction, including those determining standards, and we have shown that the effect should be included in future determinations. The NIST analysis certainly used asymmetry split Pearson VII functions to fit the peaks, but this does not address the asymmetry discussed here and may in fact amplify the error. The NIST reference did not take account of any such asymmetry, and the uncertainty published for both Si 640b and LaB<sub>6</sub> 660 is likely to be affected by at least the discrepancy reported.

A previous study by Yoder-Short (1993) also imputed a small error in the Si 640b lattice parameter arising from the

incorrect reference wavelength used to calculate the lattice parameter. This correction has not been taken into account in this analysis because it represents a change that is several orders of magnitude smaller than the discrepancy noted here.

## 8. Conclusion

The discrepancy in the ratio of expected lattice parameters is 1.000117 (12) following Fig. 13. The lattice parameter of LaB<sub>6</sub> SRM 660 is therefore determined to be 4.156468 Å with an accuracy of 12 parts per million (p.p.m.), by reference to the defined lattice spacing of Si SRM 640b. Individual energy determinations are accurate to 6 p.p.m. or 0.0006%. A discrepancy is observed between the currently accepted value and the measured value, of 0.00048 (5) Å or nine standard deviations from the NIST reference.

The main systematic errors from the experimental geometry have been corrected for. Energy-dependent systematic errors are probed over a large energy range. The consistency of the lattice parameter across the energy shows that energy-dependent errors such as sample absorption and the energy bandpass of the beam do not affect the result.

The discrepancy is consistent over the energy range 10–20 keV, ruling out energy-dependent systematic errors as its cause. Significant geometric errors have been accounted for. The lattice-parameter discrepancy is not explained by asymmetric broadening of the peaks; rather this asymmetric broadening reduces the apparent discrepancy when it is not corrected for.

Peak broadening is shown to be dominated by the beam energy bandpass at high angles. The main physical causes of broadening are identified and corrected for by deconvolution.

By determining the lattice parameter from the peak central positions, possible significant effects of peak amplitude modelling are avoided. This is an important advantage of using peak central positions, even in synchrotron experiments where the energy bandpass is relatively small but still remains significant. The peak central positions technique is used to obtain a highly accurate result and avoid many of the systematic errors present in synchrotron experiments, but must in fact be augmented by a direct investigation of the profile asymmetry for high-accuracy work.

Many researchers are primarily concerned with structural determination from powder studies; and many determine the lattice constants and beam energies using a standard powder comparison. This research clarifies uncertainties and accuracies relating to this procedure and yields a new result for general researchers.

Common peak broadening models used in Rietveld analyses have additional, correlated, free parameters including amplitude and strain coefficients. Fitting these correlated parameters yields coefficients with unphysical values, which is explicitly not observed in our high-accuracy data. Broadening due to particle size is not observed to be significant in this investigation, and its inclusion in the model can also lead to correlated and unphysical coefficients.

The present result is consistent in sign and magnitude with the previous result of Chantler *et al.* (2004). This work is a significant advance on that previous work. The best accuracy in terms of  $|\delta 2\theta|$  and individual energy determinations has been improved. All peaks are fitted, unlike earlier work and work by Hart *et al.* (1990), which excluded significant low-order peaks and measured relatively few peaks. The determination of  $\delta y$  and  $\delta z$  is more stable, more robust, and more explicitly physical across energy. Correct first-order allowance for the asymmetry has been made. The variation of consistency of the discrepancy with energy has required that the central energy data be reported as a highly accurate determination. This implies that a residual systematic remains in the data; this is most likely due to additional profile asymmetry, and would be expected to yield a more consistent and reliable result after such further correction. Of course, such a determination will require further careful experiments.

Hence this result currently represents the best determination of the lattice parameter of LaB<sub>6</sub> 660. Future work must continue this effort for all accurate powder diffraction determinations and in particular must consider the newer standards 640c and 660a.

## APPENDIX A

### Other approaches to peak profile broadening

Some previous studies have found correlation between fitting parameters when too many correlated parameters are included. In relation to the model used in this study, it is important to consider the other widely cited models in the literature.

A variation of equation (4) is often used in Rietveld analysis (Albinati & Willis, 1982) with arbitrary meaning for the three coefficients:

$$(\Delta 2\theta)^2 = A \tan^2 \theta + B \tan \theta + C(\Delta 2\theta_0)^2. \quad (7)$$

This equation was derived for neutron spectroscopy (Caglioti *et al.*, 1958) and has been interpreted to represent the particle size effect (Rietveld, 1969). However, the first component is indistinguishable from the effect of the energy bandpass, and the second component can represent correlation between these two effects. In almost all real X-ray investigations, the energy bandpass will dominate at high angles, as demonstrated by equation (4). This is also the case with the current data: the curvature of the plots is correctly represented by just the energy bandpass of the synchrotron beam.

The free parameters in equation (7) are not constrained to be positive, so that the  $B$  coefficient will usually become negative, especially if the transverse curvature of lines represented by  $\Delta 2\theta_{\text{HD}}$  is not corrected for. This negative value for  $B$  is almost always unphysical (representing an independent process which narrows the diffraction width).

A correlation of the energy  $E$  on a part of the capillary with the vertical angle incident upon that part of the powder sample is possible, and would yield a correlated coefficient ( $B$ ), which could be negative; but then  $B$  would have a

different sign for peaks above the axis of the capillary *versus* the symmetric peaks below that axis, on the opposite side of the diffracting circle. In our data, such a correlation is not observed and after correction for  $\Delta 2\theta_{\text{HD}}$ , both functions returned similar  $\chi_r^2$  values with a  $B$  coefficient consistent with zero within uncertainty. For example, in Fig. 9,  $\chi_r^2$  values were 4.26 and 4.54 for the two cases. Most of this  $\chi_r^2$  is given by one outlier, which does not affect the fit.

Another function commonly used in powder diffraction, including in the determination of the current SRM powder standards (Rasberry *et al.*, 1989; Cheary & Coelho, 1992), accounts for the particle size effect in the following manner:

$$(\Delta 2\theta) = A \tan \theta + B / \cos \theta. \quad (8)$$

This formula is not supported by our data. The coefficient  $A$  of the energy dispersion term is negative when fitted (poorly), and  $A^2$  could correspond to the  $(\Delta E/E)^2$  of the simpler models. Since the particle size term should be uncorrelated with the energy bandpass, the correlation should be orientationally dependent and hence average to zero for a spinning sample. Indeed, if this negative implies a narrowing of the width due to the bandpass of the beam, then it must be unphysical.

Dynamical diffraction broadening has been neglected in this discussion, because image-plate and pixel broadening dominates over the intrinsic width. The key exception to this is the case of the lowest order reflection. This dynamical broadening of the lowest order peaks was looked for but was negligible in the analysis. Hence all significant physical sources of broadening have been assessed and the results of this fitting procedure yield physical, stable and accurate results for the width functionality.

The authors acknowledge the experimental team and the local ANBF staff, particularly James Hester, as well as funding from the Australian Synchrotron Research Program and Australian Research Council. The authors acknowledge with

great gratitude the careful comments and assistance of Associate Professor Zwi Barnea in the experimental work and review of this paper, and acknowledge with thanks the helpful comments of the referee.

## References

- Albinati, A. & Willis, B. T. M. (1982). *J. Appl. Cryst.* **15**, 361–374.
- Ávila-Godoy, R., Mora, A. J., Acosta-Najarro, D. R., Delgado, G. E., López-Rivera, S. A., Fitch, A. N., Mora, A. E. & Steeds, J. W. (2006). *J. Appl. Cryst.* **39**, 1–5.
- Barnea, Z., Creagh, D. C., Davis, T. J., Garrett, R. F., Janky, S., Stevenson, A. W. & Wilkins, S. W. (1992). *Rev. Sci. Instrum.* **63**, 1069–1072.
- Caglioti, G., Paoletti, A. & Ricci, F. P. (1958). *Nucl. Instrum. Methods*, **3**, 223–228.
- Chantler, C. T., Tran, C. Q., Barnea, Z., Paterson, D. & Cookson, D. J. (2003). *Phys. Rev. A*, **67**, 042716(1–15).
- Chantler, C. T., Tran, C. Q., Barnea, Z., Paterson, D., Cookson, D. J. & Balaic, D. (2001). *Phys. Rev. A*, **64**, 062506(338–346).
- Chantler, C. T., Tran, C. Q. & Cookson, D. J. (2004). *Phys. Rev. A*, **69**, 042101(1–11).
- Cheary, R. W. & Coelho, A. (1992). *J. Appl. Cryst.* **25**, 109–121.
- Cookson, D. J. (1998). *J. Synchrotron Rad.* **5**, 1375–1382.
- Hart, M., Cernik, R., Parrish, W. & Toraya, H. (1990). *J. Appl. Cryst.* **23**, 286–291.
- Hastings, J., Thomlinson, W. & Cox, D. (1984). *J. Appl. Cryst.* **17**, 85–95.
- Parrish, W., Wilson, A. J. C. & Langford, J. I. (1999). *International Table for X-ray Crystallography*, Vol. C, §5.2.10. Amsterdam: Kluwer Academic.
- Rae, N. A., Chantler, C. T., Tran, C. Q. & Barnea, Z. (2006). *Radiat. Phys. Chem.* In the press.
- Rasberry, S., Hubbard, C., Zhang, Y. & McKenzie, R. (1989). *National Institute of Standards and Technology SRM Certificates, Standard Reference Materials 660*. Report, National Institute of Standards and Technology.
- Rietveld, H. M. (1969). *J. Appl. Cryst.* **2**, 65–71.
- Sabine, T. M. (1987). *J. Appl. Cryst.* **20**, 23–27.
- Sabine, T. M., Kennedy, B. J., Garrett, R. F., Foran, G. J. & Cookson, D. J. (1995). *J. Appl. Cryst.* **28**, 513–517.
- Yoder-Short, D. (1993). *J. Appl. Cryst.* **26**, 272–276.